JOURNAL OF MATERIALS SCIENCE 35 (2000) 3767–3784

CoNi and FeCoNi fine particles prepared by the polyol process: Physico-chemical characterization and dynamic magnetic properties

Ph. TONEGUZZO
CEA, Le Ripault, BP 16, F-37260 Monts, France

G. VIAU
Laboratoire de Chimie des Matériaux Divisés et Catalyse, Université Paris 7-Denis Diderot, 2 Place Jussieu, F-75251 Paris Cedex 05, France

O. ACHER, F. GUILLET, E. BRUNETON
CEA, Le Ripault, BP 16, F-37260 Monts, France

F. FIEVET-VINCENT, F. FIEVET*
Laboratoire de Chimie des Matériaux Divisés et Catalyse, Université Paris 7-Denis Diderot, 2 Place Jussieu, F-75251 Paris Cedex 05, France
E-mail: fievet@ccr.jussieu.fr

Spherical and monodisperse Co_xNi_{100-x} and $Fe_z[Co_xNi_{100-x}]_{1-z}$ particles are synthezied by the polyol process over a wide size range (lying from a few micrometers to a few tens of nanometers). The whole physico-chemical characterizations, i.e. dark-field image by TEM, SAED, density, saturation magnetization and chemical analysis, are consistent with a "core-shell" model. In the Co_xNi_{100-x} system, the particles are constituted by a ferromagnetic, almost pure and dense core surrounded by a thin coating composed of metal oxides and metallo-organic phases. On the contrary, in the $Fe[Co_xNi_{100-x}]_{1-z}$ system, the ferromagnetic core is polycrystalline, slightly porous and retains impurities in higher content, the superficial layer having almost the same composition as in the Co-Ni system, but being twice more thick. The microwave permeability of the Co_xNi_{100-x} and $Fe_z[Co_xNi_{100-x}]_{1-z}$ particles, previously insulated by a superficial treatment and then mechanically compacted, is investigated in the 100 MHz-18 GHz frequency range. Whatever the composition, submicrometer-sized particles show several narrow resonance bands which are interpreted as non uniform exchange resonance modes. Iron-based particles have lower resonance frequencies than iron-free powders; they also have higher permeability levels despite their lower cristallinity and their higher impurity content. A mild thermal treatment allows to increase this permeability by eliminating the metallo-organic impurities without modifying the morphology of the particles.

1. Introduction

The physico-chemical properties of well-defined finely dispersed metals make them of interest for many novel uses in the technology of advanced materials [1] or as model materials for fundamental studies [2]. This is especially true for ferromagnetic metals because magnetic properties are strongly dependent on particle shape and size, elemental composition and surface oxidation. Fine ferromagnetic particles are used as advanced materials in various technical fields such as magnetic recording media, ferrofluids [3], magnetic inks, sensors [4], powder metallurgy [5]. Regarding the application, the synthesis of particles with a definite shape, a tailor-made size and a narrow size distribution may be the main goal as well as the synthesis of alloyed particles with a definite composition either as crystals or amorphous phases. The physical properties of nanoscale ferromagnetic metal particles are especially the object of intensive reseach today.

For these various purposes and regarding the desired particle size range, a very wide variety of methods are used including vapor deposition [6], electrodeposition [7], solvated metallic atoms deposition [8], spray pyrolysis [9], sonochemical synthesis [10], decomposition of organometallic precursors [11], reduction from homogeneous solutions [12, 13] and in microemulsions [14, 15].

* Author to whom all correspondence should be addressed.

Among the latter chemical methods, the polyol process [16, 17], in which the liquid polyol acts both as a solvent of the metallic precursors and as a mild reducing medium, is a suitable route for the synthesis of ferromagnetic metal particles with a quasi spherical shape and a narrow size distribution. Moreover this method allows an accurate and reproducible control of the mean diameter of the particles in a broad size range lying from a few tens nanometers to a few micrometers. The polyol process allows as well to make polymetallic particles where two or three of the ferromagnetic metals (Fe, Co, Ni) are associated in various proportions. Such fine particles dispersed in an insulating matrix with a volume concentration lower than the percolation one are particularly suitable to make composite magnetic materials (also called granular materials) showing absorbing properties in the microwave range. Their remarkable well-defined morphological characteristics have allowed us lately to evidence the main role of the size of the magnetic particles upon the microwave permeability and consequently upon the absorbing properties of the composite material made up with these particles [18–21].

Moreover by varying the composition, one can expect to get particles with different magnetic properties, not only due to the influence of elemental composition upon saturation magnetization, but also due to the influence of the crystalline structure and of the surface oxidation upon volume and surface magnetocrystalline anisotropies respectively. The scope of the present study is to investigate on metal particles with well-defined morphological, textural and structural characteristics, the influence of these factors upon the microwave properties of these particles beyond the main influence of their size which has been reported recently. Such a study would allow to optimize the absorbing properties of granular materials made up with such magnetic inclusions.

2. Experimental

2.1. Particles synthesis and composite material preparation

According to the polyol process, Co_xNi_{100-x} and $Fe_z[Co_xNi_{100-x}]_{1-z}$ fine particles have been synthesized by precipitation from metallic salts dissolved in polyols. Sodium hydroxide was added in excess in order to favor the formation of solid intermediate phases such as polymetallic hydroxides or/and alkoxyde hydroxide acting as a reservoir for the metal solvated species prior their reduction into metal. Such a control of the metallic species concentrations allows to make monodisperse metal particles through a control of the growth step of these particles [16–19]. Upon heating both Co^{II} and Ni^{II} were quantitatively reduced by the polyol itself whereas Fe was generated by disproportionation of Fe^{II}. The accurate and reproducible control of the mean diameter of the particles can be achieved in the submicrometer and the nanometer size range as well, by heterogeneous nucleation for both Co_xNi_{100-x} and $Fe_z[Co_xNi_{100-x}]_{1-z}$ systems. Cations of noble metals being easily reduced by polyols, the seeding of the reaction medium was achieved by using a noble metal salt in order to generate *in situ* numerous tiny metal particles which then acted as suitable sites for the further growth of the ferromagnetic metals.

According to these guide lines, the detailed experimental procedure was as follows. Co_xNi_{100-x} and $Fe_z[Co_xNi_{100-x}]_{1-z}$ powders were prepared from cobalt(II) and nickel(II) acetate tetrahydrates and iron(II) chloride tetrahydrate (Prolabo) dissolved with sodium hydroxide (Prolabo) in 3.5/l of 1,2-propanediol (Merck). The metal concentration $[Fe^{2+}] + [Co^{2+}] + [Ni^{2+}]$ was fixed to 0.1 mol l^{-1}, the sodium hydroxide concentration being 0.25 mol l^{-1} and 1 mol l^{-1} for CoNi and FeCoNi powders respectively. Heterogeneous nucleation was achieved by adding a small amount (maximum volume 15 ml) of a solution of K_2PtCl_4 (Strem Chemicals) or $AgNO_3$ (Prolabo) dissolved in a mixture of 1,2-ethanediol and dihydroxydiethylether (1/1 vol.). The solution containing all the rectants and the nucleating agent was slowly heated up to the boiling point under mechanical stirring at 250 RPM and then maintained at this temperature during ca. 2 hours. Water and volatile organic products generated by the overall reaction were distilled off while the polyol was refluxed, the distillate being typically 10% of the total volume. After cooling, the precipitated metallic powder was separated from the liquid by decantation and then centrifugation, sonicated and washed several times with ethanol, water and acetone and finally dried under argon at 50°C.

In order to investigate their dynamic electromagnetic properties (permittivity $\varepsilon(\omega)$ and permeability $\mu(\omega)$), the metal particles have to be electrically insulated. This can be done by coating the particles with a few nanometer thick oxide layer formed by a superficial oxidation [22] or by a chemical treatment [1, 23, 24]. In our case, the coating of the metal particles with a thin dielectric manganese oxide layer was achieved according to Kocon *et al.* [25] by a soft chemical treatment in solution: 10 g of the metal powder were dispersed and sonicated at room temperature under mechanical stirring in 500 ml of a 0.25 M aqueous solution of potassium permanganate (Carlo Erba); 15 ml of a 0.5 M solution of nitric acid were admixed to the suspension. Twenty minutes later, the powder was recovered by centrifugation, washed and sonicated several times with water and acetone and finally dried in air for several hours at 60 °C. Then, these insulated particles were compacted mechanically. The main advantage of this method is to provide a composite having a high volume concentration of magnetic inclusions without any electric percolation. It has been shown [18] that a thermal treatment allows to increase the imaginary part of the magnetic permeability of the powders and therefore allows to improve the characteristics of the compacted composite material. These thermal treatments of the insulated particles were conducted in a rotating furnace under an argon flow (30 l h^{-1}) with a low heating rate (0.5 to 1 °C min^{-1}) and two plateaus at 120 °C (2 h) and 350 °C (20 h).

2.2. Powders characterization

The morphological characteristics of the particles were determined by scanning electron microscopy (SEM, Leica Stereoscan 440) and by transmission electron

microscopy (TEM), using either a Philips CM12 or a Jeol CXII apparatus. The mean diameter (d_m), and standard deviation (σ) of the size distribution were estimated from image analysis of ca. 200 particles (Microvision software). The sphericity S of each particle was calculated as follows: $S = 4\pi A P^{-2}$ with A the area of the 2D image of the particle and P its perimeter.

Phase analysis was performed by X-ray diffraction (XRD) using a D-500 Siemens X-ray powder diffractometer (Co K_α radiation $\lambda = 1.789$ Å). The lattice parameter of the cubic solid solutions was inferred by extrapolation against $(\cos^2\theta/\sin\theta)$ [26], the diffractometer being calibrated with a highly crystalline silicon powder as an external standard. The respective contribution of crystallite size and microstrains to line broadening was inferred from the half-maximum width of at least four lines using the Williamson and Hall method [27].

Chemical analysis was performed by X-ray fluorescence (XRF) using a Siemens SRS 303 apparatus or by Inductive Coupled Plasma-Atomic Emission Spectroscopy (ICP-AES). Local analysis on dispersed particles was performed by energy dispersive X-ray spectroscopy (EDS) with a nanoprobe associated with a scanning transmission electron microscope (STEM). Organic impurities contents (C, O and H) were inferred from the gas evolved during the thermal treatment of the samples in an induction oven, these contents being determined using infrared spectroscopy analyzers working at fixed wavelengths (Leco CS 244, Leco TC 436) or a thermal conductivity cell (Leco RH 404).

Real density was determined by helium pycnometry (Micromeritics Accupyc 1330). Thermogravimetry Analysis, TGA, (Setaram TG92) and Temperature Programmed Desorption (TPD) coupled with a mass spectrometer (MS) sometimes associated with a Gas Phase Chromatograph (GPC) were conducted under an argon (TGA) or an helium flow (TPD) with a 10 °C min^{-1} heating rate.

Saturation magnetization was obtained from room temperature hysteresis loop measurements using a hysteresysmeter (SIIS M2000) whereas evolution of magnetization with temperature was followed with a magnetic balance (Manics DSM). In order to investigate their microwave properties, the insulated particles were mechanically compacted in a brass coaxial cell. $\varepsilon(\omega)$ and $\mu(\omega)$ were measured on this composite material in the 100 MHz-18 GHz frequency range with a APC7 coaxial line associated with a HP 8510 network analyzer. As detailed elsewhere [21], the intrinsic particle permeability, μ_i, was calculated from these measurements, the metal volume concentration being inferred from density and saturation magnetization measurements.

3. Powder characteristics

3.1. Morphological characteristics

Co_xNi_{100-x} and $Fe_z[Co_xNi_{100-x}]_{1-z}$ powders obtained by precipitation in polyols are made up of quasi-spherical and non-agglomerated particles with a very narrow size distribution (Figs 1 and 2). The deviation from an ideal spherical shape is very small for iron-based particles (typically $S = 0.99$) whereas it is slightly larger for CoNi particles ($S = 0.80$). Chain-like arrangements are often observed by TEM with the finest powders due to dipolar interactions between neighboring particles. An accurate and reproducible control of the mean diameter d_m can be achieved through heterogeneous nucleation [19–21]. Hence, d_m is varied from a few micrometers (through spontaneous nucleation) to 25 nm (heterogeneous nucleation by seeding with Pt). Whatever the composition or the mean particle size, the standard deviation σ of the size distribution is systematically lower than 15% d_m, and even lower than 10% d_m for $Fe_z[Co_xNi_{100-x}]_{1-z}$ powders. In every cases the histogram appears symmetrical. These powders can be considered as monodisperse systems except for the particular composition Fe_zCo_{100-z} for which the samples always appear as agglomerated particles with an irregular shape.

Furthermore, it must be stressed that the morphological characteristics of the powders are retained after the coating of the particles with an insulating manganese oxide layer and after the subsequent annealing treatment as exemplified in Fig. 3. The coating oxide layer appears thick enough (about 10 nm) to prevent sintering during the thermal treatment provided this treatment is conducted under suitable conditions namely in a rotating furnace, under a neutral atmosphere, at a low temperature and a low heating rate (see experimental section). The oxide layer remains homogeneous and adherent after annealing. Whereas d_m remains constant upon annealing for Co-Ni particles, it slightly decreases for iron-based particles. For instance for a $Fe_{0.13}[Co_{50}Ni_{50}]_{0.87}$ composition, d_m decreases from 215 nm to 200 nm, whereas the standard deviation σ remains equal to 20 nm and the sphericity equal to 0.99 (Fig. 3a and b).

3.2. Chemical analysis

3.2.1. Metals

The chemical analysis of Co_xNi_{100-x} and $Fe_z[Co_xNi_{100-x}]_{1-z}$ powders showed that for the former the Co/Ni molar ratio was very close to the ratio of the corresponding cations in the starting solution, whereas for the latter the Fe/M molar ratio (M = Co, Ni) was significantly lower. This result confirms that the yield of formation of iron is indeed limited by the disproportionation of Fe^{II}, Fe^{III} being retained in solution. Co^{II} and Ni^{II} are on the contrary quantitatively reduced. Hence polymetallic powders can be synthesized with z and x varying in the range 0–0.25 and 0–100 respectively. It must be stressed than ions of electropositive metals, namely Na^+, are retained in solution, the corresponding metal content in the final powder being very low whatever its content in the starting material.

The metal ratio measured by EDS by analyzing several particles was quite identical to the global composition measured by XRF or ICP-AES. Then, a good interparticular homogeneity in composition is ascertained for both Co_xNi_{100-x} and $Fe_z[Co_xNi_{100-x}]_{1-z}$ powders.

Except for Fe_zCo_{100-z} powders whose particles are made up of an iron core surrounded by cobalt [17], no segregation of the different metals was observed by

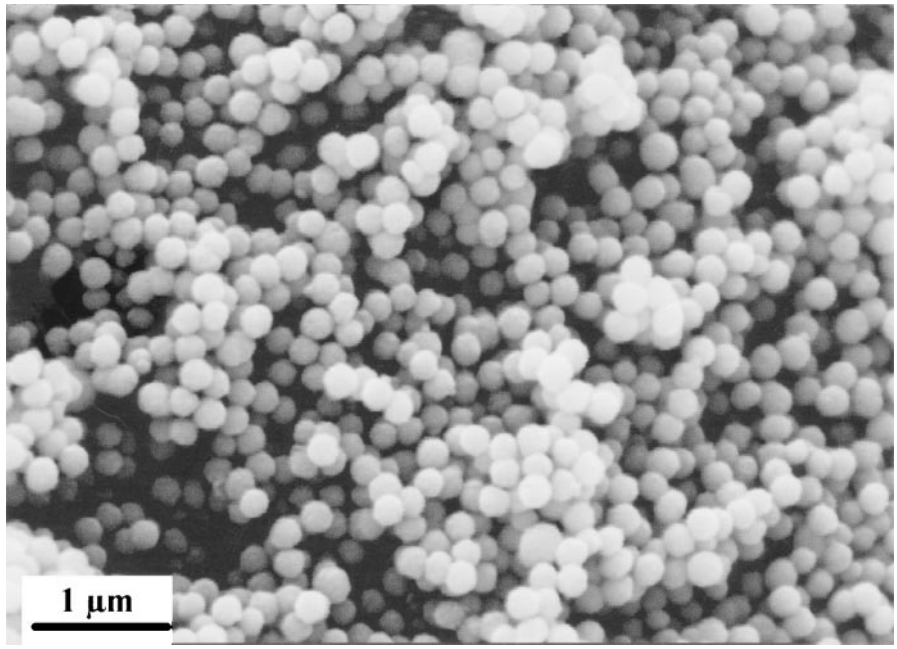

(a)

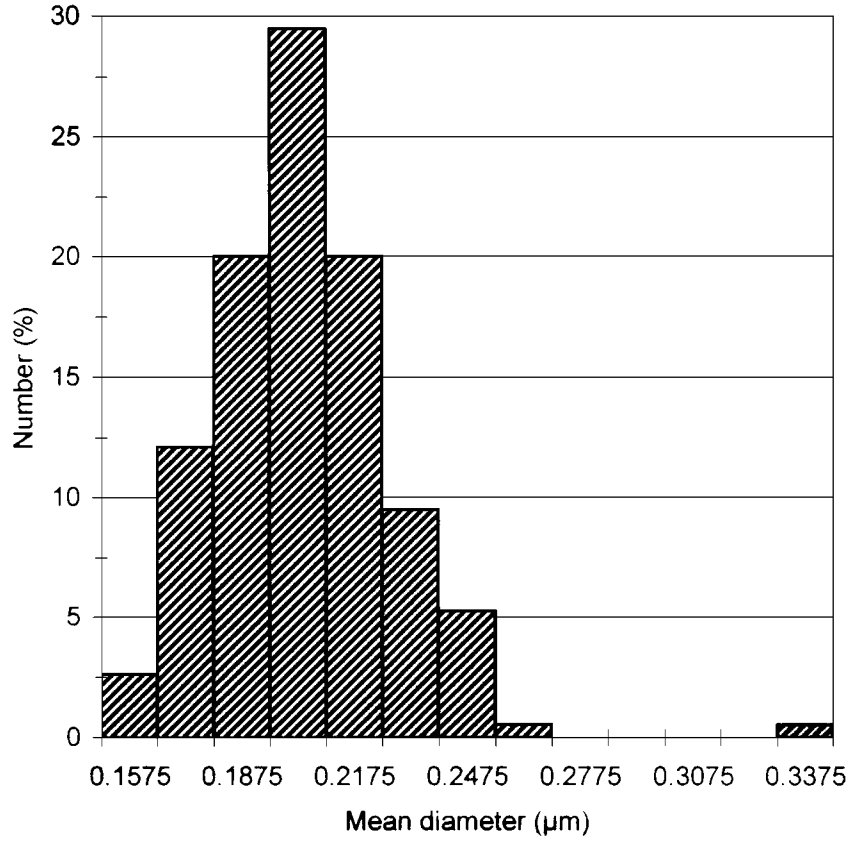

(b)

Figure 1 (a) SEM image of $Fe_{0.13}[Co_{80}Ni_{20}]_{0.87}$ particles ($d_m = 205$ nm, $\sigma = 25$ nm) and (b) histogram of size distribution.

EDS analysis in the distribution maps of the elements. Nevertheless, as exemplified in Table I, a concentration gradient for Ni and Co could be shown for both Co_xNi_{100-x} and $Fe_z[Co_xNi_{100-x}]_{1-z}$ powders by fixing the nanoprobe (ca.10 nm of diameter for the highest magnification) at the core and at the edge on an isolated particle. Such an analysis which is used usually on flat surfaces, does not provide the exact metal composition of the core of a spherical particle. Indeed, the analyzed volume includes the core and the surface as well when the probe is located at the center of the particle. Nevertheless, the significant and reproducible changes in composition observed on single particles versus the probe position allows to draw a qualitative conclusion: the core of the particles is always richer in Co and poorer in Ni than the edge, for both CoNi and FeCoNi systems whatever the chemical composition and the mean size of the particles. In contrast, Fe appears to be rather homogeneously distributed within each particle. Moreover, it must be pointed out that the

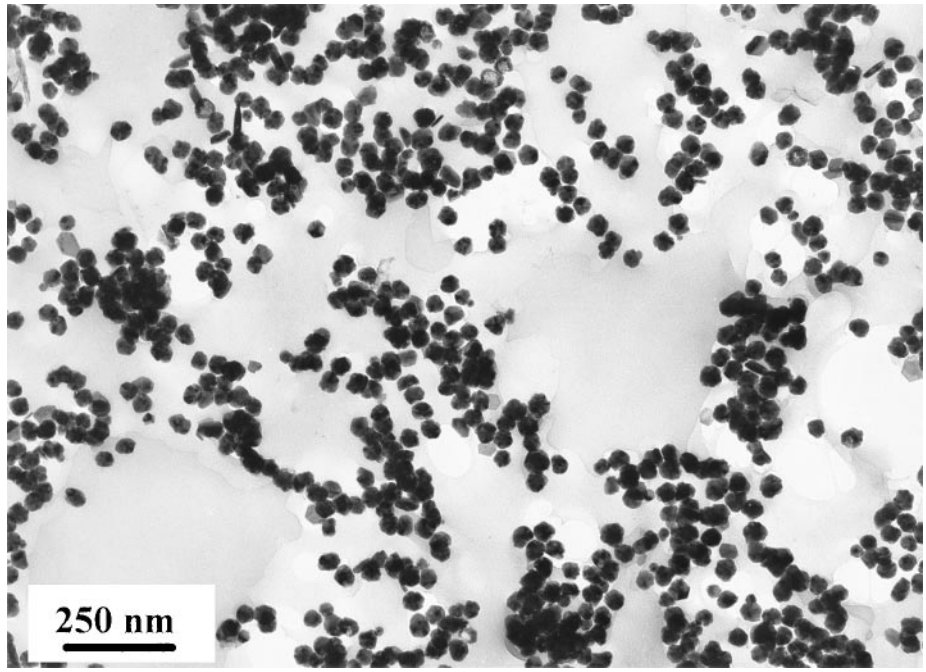

(a)

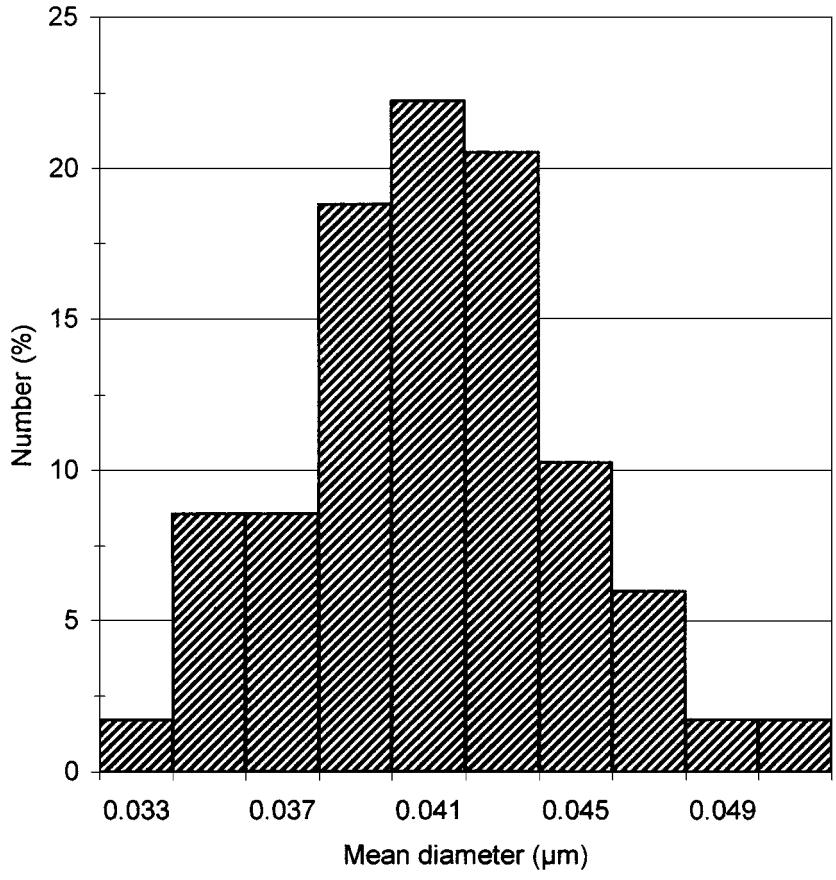

(b)

Figure 2 (a) TEM image of $Co_{65}Ni_{35}$ particles ($d_m = 42$ nm, $\sigma = 5$ nm) and (b) histogram of size distribution.

intraparticular Co-Ni gradient is still evidenced by EDS after the annealing treatment conducted at 350°C.

3.2.2. Non metallic impurities

As expected for finely divided powders synthesized in boiling organic medium the main impurities are carbon, oxygen and hydrogen. Typical C and O contents are exemplified in Table II for samples with a similar particle size (ca. 220 nm) and different compositions, in both the Co-Ni and Fe-Co-Ni systems. For this latter system these impurities contents are always significantly higher than in the former for which a slight decrease is observed when x decreases from 100 to 20. For both systems, the carbon and oxygen contents increase steadily when the mean particle size decreases, then

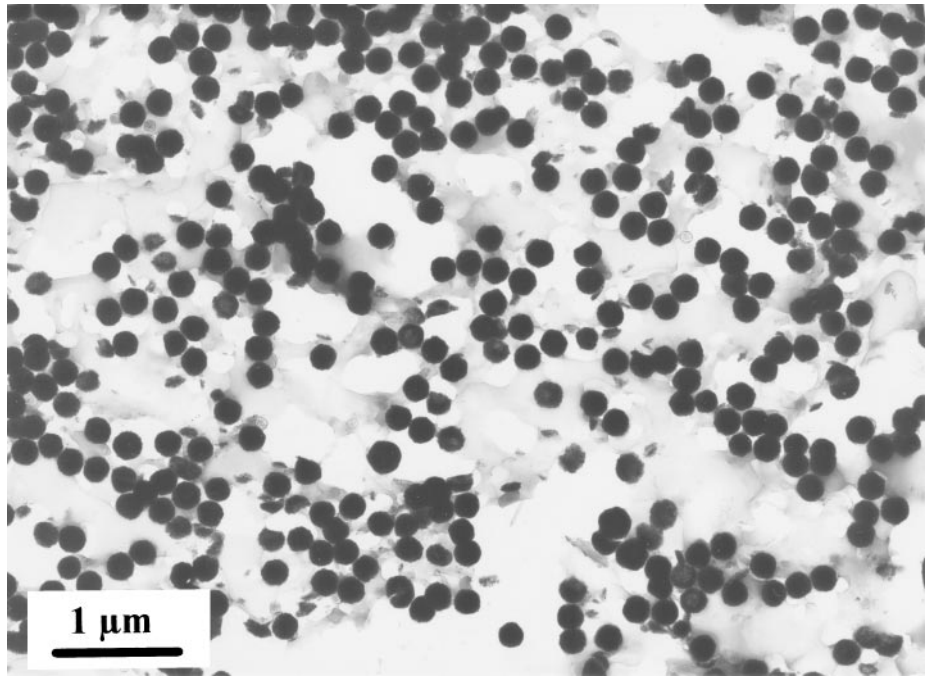

(a)

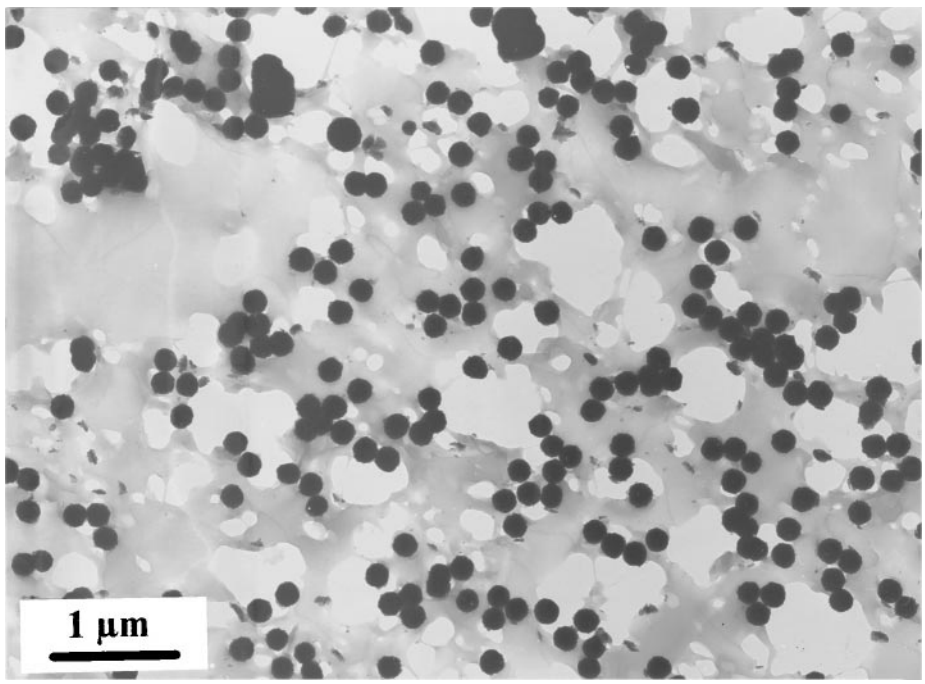

(b)

Figure 3 TEM image of $Fe_{0.13}[Co_{50}Ni_{50}]_{0.87}$ particles prepared by the polyol process by heterogeneous nucleation (Pt): (a) after superficial treatment ($d_m = 215$ nm; $\sigma = 20$ nm); (b) after superficial treatment and annealing under argon ($d_m = 200$ nm; $\sigma = 20$ nm).

TABLE I Relative composition (at. %) measured by microanalysis with a broad nanoprobe (global analysis) or a fixed nanoprobe (punctual analysis on the edge or on the center of a particle)

	Fe (at. %)	Co (at. %)	Ni (at. %)	Co/Ni
Area of several particles	14	42	44	0.95
	15	41	43	0.95
Single isolated particle "center"	16	47	37	1.27
	15	50	35	1.43
Single isolated particle "edge"	13	39	48	0.81
	10	36	54	0.67

it may supposed that these impurities are mainly located at the surface of the particles. This point will be discussed in detail in the next paragraph.

Carbon and oxygen can originate from the presence of organic adsorbed species (either polyol or degradation products) or from a metallo-organic phase such as metal alkoxyde hydroxide observed as an intermediate phase. Moreover, oxygen can also originate from inorganic phases such as unreacted hydroxides, oxides due to the disproportionation of iron or to a superficial oxidation of the finely divided metal particles. Such assumptions are supported by TGA. Total weight

TABLE II Oxygen and carbon contents of Co_xNi_{100-x} and $Fe_{0.13}[Co_xNi_{100-x}]_{0.87}$ powders against chemical composition for samples with a similar mean particle size

Composition	x	100	80	65	50	35	20	0
$Co_xNi_{(100-x)}$	d_m (μm)	0.26	0.22	0.22	0.24	0.22	0.24	0.22
	O (wt. %)	1.7	1.4	1.2	1.1	1	0.78	1.2
	C (wt. %)	0.68	0.54	0.48	0.36	0.29	0.27	0.38
$Fe_{0.13}[Co_xNi_{(100-x)}]_{0.87}$	d_m (μm)		0.22		0.22	0.24	0.22	0.22
	O (wt. %)		4.4		3.9	3.9	4.4	3.3
	C (wt. %)		1.2		1.2	1.6	1.6	3

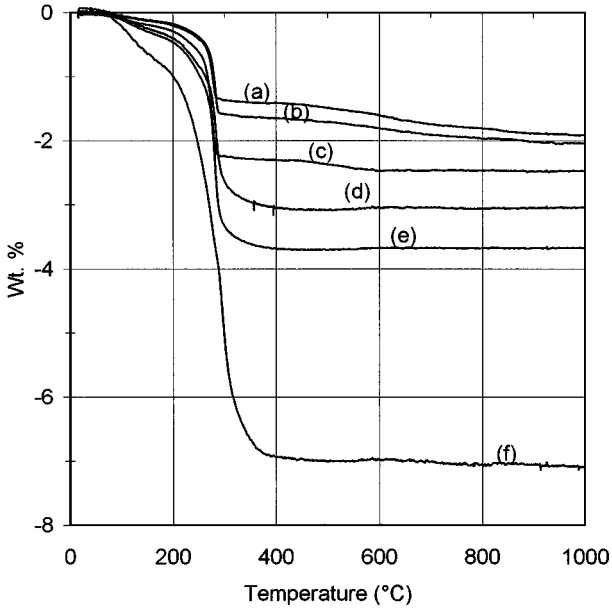

Figure 4 TGA curves under argon of $Co_{80}Ni_{20}$ powders for different mean diameter: (a) $d_m = 240$ nm; (b) $d_m = 200$ nm; (c) $d_m = 145$ nm; (d) $d_m = 80$ nm; (e) $d_m = 70$ nm; (f) $d_m = 25$ nm.

losses are consistent with the impurities levels inferred from the analysis of the gas evolved during the thermal treatment of the samples. As exemplified in Fig. 4 for $Co_{80}Ni_{20}$ samples of different particle size, the total weight loss increases as the particle size decreases. TGA curves show also that the thermal decomposition of the impurities occurs in two steps. First the minor one takes place at low temperature (about 100°C) and corresponds mainly to the removal of adsorbed water, second the major one always occurs at the same temperature (about 280°C) whatever particles size and metal composition. A qualitative and quantitative analysis by TPD and GPC shows that carbon dioxide and in a less extent water are the main gaseous compounds evolved during this second step. Furthermore, this latter step coincides with a sudden increase of the saturation magnetization. Thus this second step can be considered as the thermal decomposition of the organic moiety of the impurities, the metallo-organic phases yielding ferromagnetic metals which increases the saturation magnetization. This interpretation is supported by the fact that the alkoxide hydroxide which can be isolated as an intermediary phase during the synthesis of the metal powders, undergoes decomposition under argon in the same temperature range with formation of metals, carbon dioxide and water. The second moiety of the impurities is formed by oxides which are still present at the end of the thermal treatment under argon at 1000 °C since the O content is still a few wt.-% whereas C and H contents are very low.

The chemical analysis of the as-made powders has been completed by measurements after the coating of the particles with an insulating manganese oxide layer and after the subsequent annealing treatment (Table III). As expected, the O content is enhanced by the insulating treatment whereas the C content remains unchanged. After the subsequent annealing treatment conducted under argon at 350 °C the C content becomes as low as 0.1–0.4 wt.-% for $Fe_z[Co_xNi_{100-x}]_{1-z}$ samples and even lower than 0.15 wt.-% for Co_xNi_{100-x} ones, whereas the O content falls in the range 2–3 wt.-% and 3–4.5 wt.-% for Co_xNi_{100-x} and $Fe_z[Co_xNi_{100-x}]_{1-z}$ powders respectively. It appears that a mild thermal treatment conducted at 350°C is able to remove the organic impurities. At such a temperature the remaining oxide layer of the as-prepared particles is not thick enough to prevent their sintering whereas it is avoided if the particles are coated with the insulating manganese oxide layer. It may also be pointed out that this insulating manganese oxide layer allows to decrease markedly

TABLE III Oxygen and carbon contents of Co_xNi_{100-x} and $Fe_{0.13}[Co_xNi_{100-x}]_{0.87}$ powders for different compositions: (a) as-made powders; (b) superficially treated powders; (c) superficially treated and annealed powders

	(a)		(b)		(c)	
Composition	O (wt. %)	C (wt. %)	O (wt. %)	C (wt. %)	O (wt. %)	C (wt. %)
$Co_{20}Ni_{80}$	0.88	0.27	3.8	0.31	2.3	0.05
$Co_{35}Ni_{65}$	1.0	0.36	3.8	0.40	2.1	0.07
$Co_{50}Ni_{50}$	1.1	0.36	4.1	0.36	2.6	0.08
$Co_{65}Ni_{35}$	1.2	0.48	4.7	0.54	2.3	0.13
$Fe_{0.13}[Co_{20}Ni_{80}]_{0.87}$	4.4	1.6	7.3	1.5	4	0.34
$Fe_{0.13}[Co_{35}Ni_{65}]_{0.87}$			8.4	1.4	3.7	0.15
$Fe_{0.13}[Co_{50}Ni_{50}]_{0.87}$	8.2	1.7	11.6		4.3	
$Fe_{0.13}[Co_{80}Ni_{20}]_{0.87}$	3.5	1.5	6	1.4	3.2	0.25

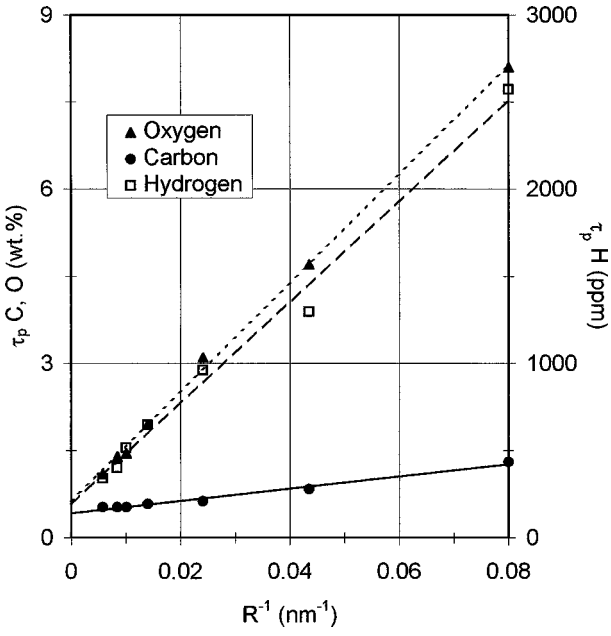

Figure 5 C, O and H contents (wt. %) vs. the reciprocal of the particles mean radius R for a given composition ($Co_{80}Ni_{20}$).

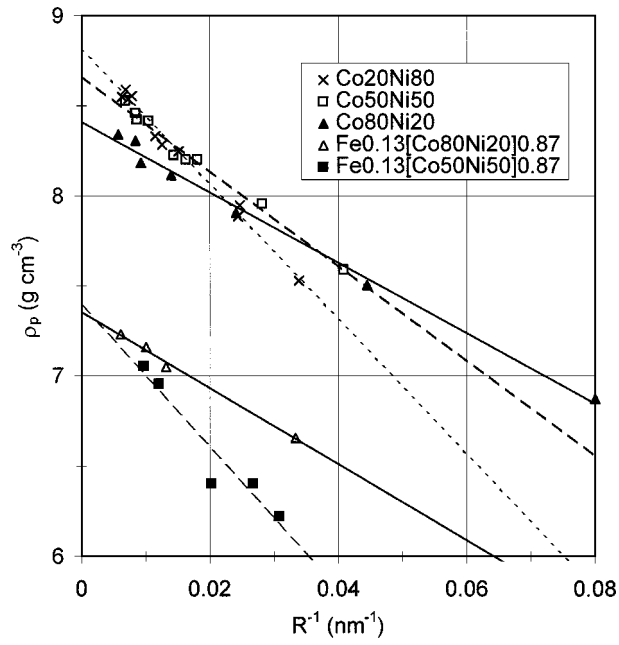

Figure 6 Real density ρ of $Co_{20}Ni_{80}$, $Co_{50}Ni_{50}$, $Co_{80}Ni_{20}$ and $Fe_{0.13}[Co_{50}Ni_{50}]_{0.87}$ powders vs. the reciprocal of particles mean radius R.

the oxidation rate of the metal particles under an oxidative atmosphere at 400 °C.

3.3. Observation of a "core-shell" texture

As it has been said, non metallic impurities contents increase steadily when the mean particle size decreases for a given composition for both Co-Ni and Fe-Co-Ni systems. Moreover, if experimental C, O and H contents are plotted against the reciprocal of the mean radius of the particles inferred from image analysis, a linear relationship is obtained with a very good coefficient of linear regression as exemplified for $Co_{80}Ni_{20}$ in Fig. 5.

A similar linear relationship is observed with density measurements conducted by helium pycnometry (Fig. 6) and with saturation magnetization inferred from hysteresis loop measurements (Fig. 7) for each composition in both Co_xNi_{100-x} and $Fe_{0.13}[Co_xNi_{100-x}]_{0.87}$ systems. A steady decrease of saturation magnetization of ferromagnetic particles against their size have been often reported in the literature [28–31] and explained by the presence of a thin metal oxide layer whose volume fraction increases as the particles radius decreases. Nevertheless, for the finest particles the significant discrepancy between experimental results and theoretical calculations has been noticed and related to spin pinning or canting [32, 33].

The linear relationships of impurities contents, density and saturation magnetization against particle size observed in the present study are also explained by a core-shell model. It is assumed that all the particles of a given sample are spherical, with the same radius (reasonable hypotheses owing to the measured sphericity and the narrowness of the size distribution) and are made up of a core which is mainly (but *a priori* not exclusively) constituted by ferromagnetic metals and a thin coating layer of impurities. This coating layer which is made up by the metallo-organic and oxide

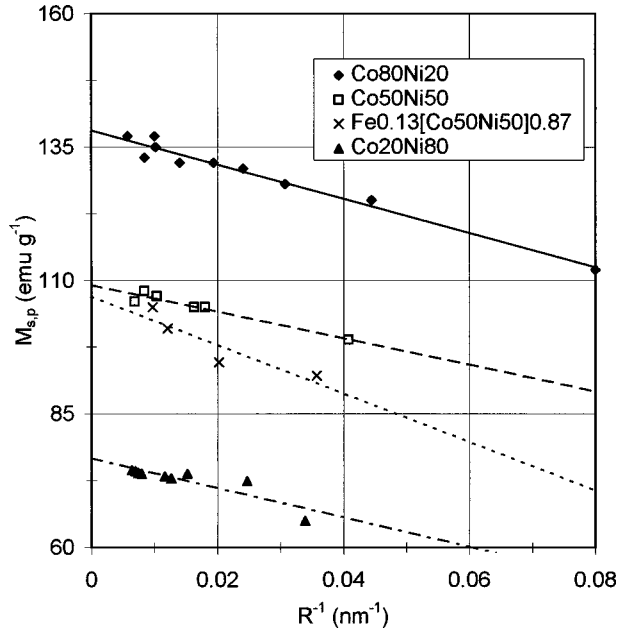

Figure 7 Saturation magnetization M_s of $Co_{20}Ni_{80}$, $Co_{50}Ni_{50}$, $Co_{80}Ni_{20}$ and $Fe_{0.13}[Co_{50}Ni_{50}]_{0.87}$ powders vs. the reciprocal of particles mean radius R.

phases as inferred from chemical analysis, is obviously less dense and has a lower magnetization than the core. Then, the increase of the overall impurities contents, the decrease of the density and of the saturation magnetization with decreasing particle size is explained by the increase of the relative volume fraction of this layer assuming that its thickness is constant. From these hypotheses the following equations can be written:

$$\tau_p m_p = \tau_c m_c + \tau_l m_l \quad (1a)$$

$$\rho_p V_p = \rho_c V_c + \rho_l V_l \quad (1b)$$

$$M_{s,p} m_p = M_{s,c} m_c + M_{s,l} m_l \quad (1c)$$

TABLE IV Density ρ, saturation magnetization M_s, impurity (carbon and oxygen) content τ of the core of particles of different compositions; the experimental values are inferred from Equation 2a–c and compared with bulk data

	ρ_c (g cm^{-3})	ρ_{bulk} (g cm^{-3})	ρ_c/ρ_{bulk}	$M_{s,c}$ (emu g^{-1})	$M_{s,bulk}$ (emu g^{-1})	$M_{s,c}/M_{s,bulk}$	$\tau_{c,carbon}$ (wt. %)	$\tau_{c,oxygen}$ (wt. %)
$Co_{20}Ni_{80}$	8.81	8.90	0.99	76.7	77.7	0.99	0.06	0
$Co_{50}Ni_{50}$	8.67	8.90	0.97	109.2	111.5	0.98	0.21	0.20
$Co_{80}Ni_{20}$	8.40	8.90	0.94	138.1	141.7	0.98	0.42	0.62
$Fe_{0.13}[Co_{50}Ni_{50}]_{0.87}$	7.39	>8.5	<0.87	107	125[a]	0.85[a]		
$Fe_{0.13}[Co_{80}Ni_{20}]_{0.87}$	7.36	>8.5	<0.87					

[a]bulk value is not available in the literature, it has been calculated on the assumption that the saturation magnetization linearly depends on iron content.

where τ, m, ρ, V, M_s are elemental impurity content (wt.-%) for instance C content, mass, density, volume and saturation magnetization respectively, the subscripts p, c and 1 being related to the whole particle, the core and the impurity layer respectively. Then, by introducing R the particle radius, e the layer thickness, by assuming that $e \ll R$ and that $M_{s,1} = 0$[†] the following equations are inferred after simplification by limited development:

$$\tau_p = \tau_c + 3e\frac{\rho_l}{\rho_c}(\tau_l - \tau_c)R^{-1} \quad (2a)$$

$$\rho_p = \rho_c - 3e(\rho_c - \rho_l)R^{-1} \quad (2b)$$

$$M_{s,p} = M_{s,c} - 3eM_{s,c}\frac{\rho_l}{\rho_c}R^{-1} \quad (2c)$$

These equations inferred from this textural model account for the above-mentioned experimental linear relationships observed when these quantities are plotted vs. R^{-1}. Moreover, it is shown in Equation 2a–c that the impurity content, the density and the saturation magnetization of the core can be inferred from the intercept of the different lines with the ordinate. The different values obtained for different compositions in both Co_xNi_{100-x} and $Fe_{0.13}[Co_xNi_{100-x}]_{0.87}$ systems are given in Table IV.

For Co_xNi_{100-x} powders, the core density which decreases as the cobalt content increases is never far from the bulk one, the lower value obtained for $Co_{80}Ni_{20}$ being only 6% lower than the bulk one. Whatever the metal composition in this system, the core saturation magnetization is also very close to bulk value (more than 98%). The core impurities contents which remain very weak for all compositions in the Co_xNi_{100-x} system, continuously decreases with Ni content till $Co_{20}Ni_{80}$ composition for which the impurities levels are close to 0. These variations of the impurity level can be related with the slight variation of the density with composition. All these characteristics of the CoNi powders are consistent with an almost non-porous core formed by ferromagnetic metals with a low content of non-metallic phase.

On the contrary, in the $Fe_{0.13}[Co_xNi_{100-x}]_{0.87}$ system, the core density is significantly lower than the bulk datum (more than 15%). Moreover, as exemplified for $Fe_{0.13}[Co_{50}Ni_{50}]_{0.87}$ (Table IV) the core saturation magnetization can be estimated to 85% of the bulk one. These characteristics are explained by the presence as impurities of non-metallic phases within the core of iron-based particles and by a certain porosity of this core. Gangopadhyay *et al.* [34] have inferred the saturation magnetization of the core of iron nanoparticles elaborated by an evaporation-deposition technique and coated by a thin oxide layer. They found a saturation magnetization (220 emu g^{-1}) which is identical to the bulk one.

[†]for iron-based particles the ferrimagnetic oxides maghemite and magnetite if present in the impurity layer are considered in too weak proportion to contribute significantly to the magnetization.

TABLE V Density ρ and thickness e of the layer of the particles for different compositions; the values are inferred from Equation 2b and c

	ρ_1 (g cm^{-3})	e (nm)
$Co_{20}Ni_{80}$	4.0	2.6
$Co_{50}Ni_{50}$	3.7	1.8
$Co_{80}Ni_{20}$	4.2	1.6
$Fe_{0.13}[Co_{50}Ni_{50}]_{0.87}$	3.3	3.2

Moreover, for a given sample, ρ_c and $M_{s,c}$ being known, the thickness e and the density ρ_1 of the coating non-metallic layer are inferred from the slopes of the lines of Figs 6 and 7 according to Equation 2b and c (Table V). Thus, the calculated density of the impurity layer varies slightly around 4 g cm^{-3} with metal composition for Co_xNi_{100-x} particles. This value is markedly lower than those expected for pure nickel or cobalt oxides [35] ($\rho_{NiO} = 6.72$ g cm^{-3}, $\rho_{CoO} = 6.44$ g cm^{-3}, $\rho_{Co3O4} = 6.11$ g cm^{-3}). That can not be due to an open porosity since such a porosity is not taken into account by helium pycnometry measurements. This value is consistent with a coating layer formed by a mixture of metal oxides and less dense organic or metallo-organic phases as inferred from the above-mentioned chemical analysis results. The thickness of this layer is about 2 nm in the Co_xNi_{100-x} system and is consistent with the starting assumption $e \ll R$. This layer is twice more thick for $Fe_{0.13}[Co_{50}Ni_{50}]_{0.87}$ than for $Co_{50}Ni_{50}$ particles (Table V). This thicker impurity layer and the occurrence of non-metallic impurities in the metal core account both for the higher overall impurities contents and the higher deviation from bulk values of the density and of the saturation magnetization for iron-based particles with respect to Co_xNi_{100-x} particles. Moreover, the value of the thickness layer is in good agreement with previous determinations for iron particles with a similar size. Thus, the thickness of a magnetite (or maghemite) coating on iron nanoparticles

elaborated by Hadjipanayis *et al.* is ranging from 1.2 nm to 2.2 nm, as inferred from the variation of saturation magnetization against particles size [31]. Tamura *et al.* [36] found that the oxide shell thickness of Fe particles made by a gas evaporation method is about 1.2 nm, using Mössbauer spectroscopy. Shinjo *et al.* [37] estimated the oxide shell thickness to be about 1.3 nm, this experimental value being inferred from electron spectroscopy for chemical analysis (ESCA) measurements by cleaning the surface of oxide coated Fe particles by sputtering with argon atoms. In fact, in most studies (essentially for nanoparticles elaborated by physical techniques such as evaporation-deposition method), an oxide layer is deliberately produced by controlled exposure to air in order to passivate the surface of the particles and hence prevent the pyrophoricity phenomenon. For our as-prepared-powders, the impurity layer appears in most cases thick enough to avoid this pyrophoricity phenomenon and hence it is not essential to slightly oxidize the metal powders in a controlled way prior to recover them in an air atmosphere after drying. However, the pyrophoricity occurs for the finest powders ($d_m < 25$ nm) due to their very high specific surface area ($A_s > 40$ m^2 g^{-1}).

3.4. Phase analysis and texture of the metallic core of the particles

3.4.1. Phase analysis

Whatever the composition and the particle diameter, in both Co_xNi_{100-x} and $Fe_{0.13}[Co_xNi_{100-x}]_{0.87}$ systems, crystalline metallic phases present in the core of the particles are the only phases detected by XRD (Fig. 8a and b). The metallo-organic phases and the oxide phases present in the coating layer (and in some extent in the core of iron-based powders) are never evidenced due to their low relative amount and/or their low crystallinity. The powder pattern depends on composition: a face-centered cubic (fcc) phase is always observed either as a single phase or as the main phase in both Co_xNi_{100-x} and $Fe_{0.13}[Co_xNi_{100-x}]_{0.87}$ systems, a second hexagonal close-packed (hcp) phase with weak and broad lines appears for a cobalt content $x \geq 35$ (Fig. 8a and b) and for $Fe_z[Co_xNi_{100-x}]_{1-z}$ powders a third body-centered cubic (bcc) phase can be evidenced when $x > 80$ (Fig. 8b).

In the Co_xNi_{100-x} system, the occurrence of a hcp phase for high cobalt content is in qualitative agreement with the phase equilibrium diagram [38], this hcp phase being expected for $x \geq 70$ instead of $x \geq 35$. Furthermore, the accurate determination of the lattice parameter of the fcc phase shows a linear dependence against composition over the entire metal composition range (Fig. 9). Such a linear dependence which agrees with Vegard's law has been previously reported for bulk alloys [39]. There is an increasing departure with increasing x between our experimental straight line and the theoretical line inferred from the lattice parameters [40] of bulk pure metallic Co or Ni fcc phases (Fig. 9). This can be tentatively explained by the occurrence of stacking faults when x increases; the resulting shift of the peaks leads to an apparent small variation of the lattice parameter. Nevertheless, the experimental linear relationship brings evidence of the occurrence of a fcc solid solution over the whole composition range for Co_xNi_{100-x} finely divided powders obtained through the polyol process at low temperature.

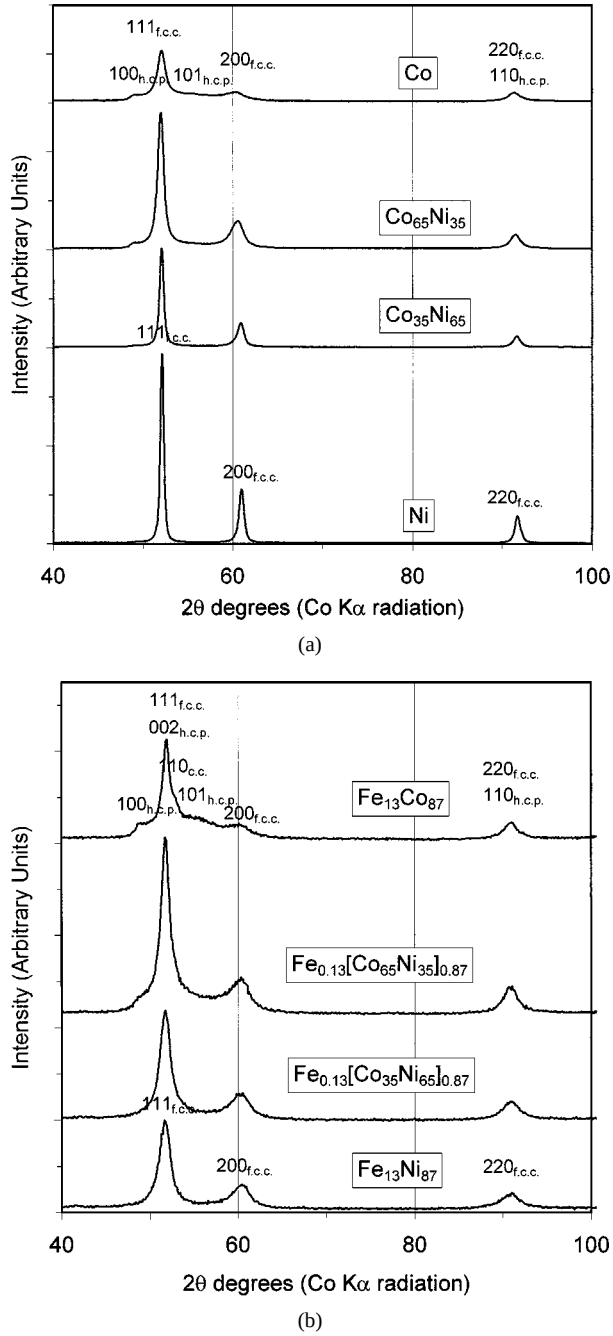

Figure 8 XRD patterns (Co K_α radiation) of powders of different compositions with an almost constant particle size: (a). Co_xNi_{100-x}; (b) $Fe_{0.13}[Co_xNi_{100-x}]_{0.87}$.

In the Fe_zNi_{100-z} system a single fcc single phase is observed over the whole available composition range ($z \leq 20$) with a linear dependence of the lattice parameter vs. z. This linear relationship already observed for bulk alloys [41] according to Vegard's law shows the existence of a fcc solid solution in the Fe_zNi_{100-z} system as early evidenced for the Co_xNi_{100-x} system. In the Fe_zCo_{100-z} system the three phases are quite similar to those of pure metals (bcc for α-Fe and a mixture of hcp and fcc phases for cobalt). This observation is consistent with the segregation of the two metals inferred from EDS measurements.

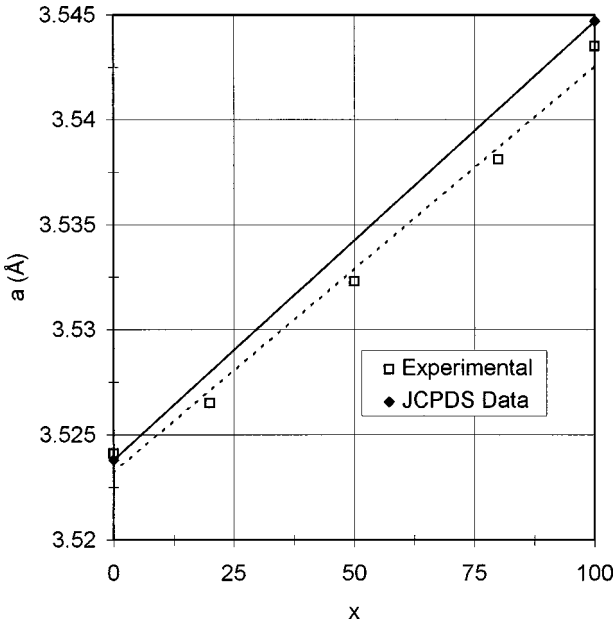

Figure 9 Linear variation of the lattice parameter of the fcc phase in the Co_xNi_{100-x} system: (dashed line) experimental; (solid line) inferred from JCPDS data for bulk pure metals.

3.4.2. Texture

In the followings, as in the previous section, texture can be defined according to Figlarz *et al.* [42] as the arrangement of the domains of matter inside the particles and namely the arrangement of the crystallites. The size of the crystallites can be either estimated from direct observation through dark-field transmission microscopy or inferred from X-ray line broadening analysis.

Dark-field TEM images show a significant difference between Co_xNi_{100-x} and $Fe_z[Co_xNi_{100-x}]_{1-z}$ particles. Each iron-based particles are made up of many crystallites whose mean size is a few nanometers (Fig. 10a and b). This is consistent with the selected area electron diffraction (SAED) pattern of an isolated particle where several continuous diffraction rings corresponding to the fcc phase are observed (Fig. 10c) whereas a weak ring corresponding to the minor hcp one is evidenced only for Co rich compositions. In contrast, Co_xNi_{100-x} particles are made up of a few bigger crystallites with a more irregular shape (Fig. 11a and b). SAED patterns confirms this texture since the fcc phase appears with spotty rings (Fig. 11c).

This difference in texture between Co_xNi_{100-x} and $Fe_z[Co_xNi_{100-x}]_{1-z}$ particles is corroborated by X-ray line broadening analysis of the lines of the fcc phase. Mean crystallite sizes are always significantly smaller for iron-based powders than for Co-Ni powders (Table VI), in both cases the mean crystallite size inferred using Williamson-Hall plot being consistent with the size of the crystallites observed on dark-field TEM image. The microstrains coefficients of Co-Ni samples increases steadily with cobalt content (Table VI). As expected annealing conducted under argon at 350 °C increases the mean crystallite size whereas the microstrains coefficient decreases significantly as exemplified in Table VI for a $Fe_{0.13}[Co_{50}Ni_{50}]_{0.87}$ sample.

This difference in texture between Co_xNi_{100-x} and $Fe_z[Co_xNi_{100-x}]_{1-z}$ powders evidenced by TEM and by X-ray line analysis as well, can also be related to the difference of porosity of the particle cores inferred from density measurements. It has been suggested elsewhere [43] that these different textural characteristics can be tentatively related to two distinct growth mechanisms. This growth may proceed either by a stepwise addition of atoms (Co-Ni particles) or by coalescence of primary particles which form secondary larger particles (iron-based particles).

TABLE VI Mean crystallite size D and microstrains coefficient η inferred from Williamson- Hall plot for Co-Ni and Fe-Co-Ni powders

Composition	D (nm)	$\eta \times 10^3$
Ni	60	5
$Co_{20}Ni_{80}$	40	8.5
$Co_{50}Ni_{50}$	65	13
$Co_{80}Ni_{20}$	40	19
Co	50	26
$Fe_{13}Ni_{87}$	15	21
$Fe_{18}Ni_{82}$	12	20
$Fe_{0.13}[Co_{50}Ni_{50}]_{0.87}$	15	15
$Fe_{0.13}[Co_{50}Ni_{50}]_{0.87}$[a]	30	10

[a]sample annealed under argon at 350 °C during 100 h.

The difference in texture between Co_xNi_{100-x} and $Fe_z[Co_xNi_{100-x}]_{1-z}$ powders is smoothed away by annealing. Whereas the coating of the particles by a dielectric layer significantly decreases the density of the powders (up to 1 g cm^{-3}) for both systems, the subsequent thermal treatment increases this density in a different extent regarding the composition (Table VII). Thus, densities of as made Co_xNi_{100-x} powders are quite the same as those of coated and annealed powders despite the presence of a low density layer of manganese oxide. On the contrary, for iron-based powders, the overall relative increase in density is currently in the range 15–20% except for Ni-rich compositions where it is smaller as exemplified in Table VII. Furthermore, XRD lines appear significantly narrower after annealing only for iron-based powders; this is due to an increase of the crystallite mean size and to a decrease of microstrains (Table VI).

4. Magnetic dynamic properties

4.1. Results

The polyol method provided samples which allow to study the microwave properties of monodisperse submicrometer sized particles with the same spherical shape and an almost equal mean diameter over a

TABLE VII Influence of coating and annealing upon the density of Co_xNi_{100-x} and $Fe_{0.13}[Co_xNi_{100-x}]_{0.87}$ powders for different compositions: (a) as-made powders; (b) superficially treated powders; (c) superficially treated and annealed powders

Composition	d_m (nm)	ρ_p (g cm^{-3}) (a)	(b)	(c)	$(\rho_{(c)} - \rho_{(a)})/\rho_{(a)}$ (%)
$Co_{20}Ni_{80}$	315	8.55	7.72	8.58	0.4
$Co_{50}Ni_{50}$	190	8.41	7.56	8.46	0.6
$Fe_{0.13}[Co_{20}Ni_{80}]_{0.87}$	225	7.14	6.57	7.76	8.7
$Fe_{0.13}[Co_{50}Ni_{50}]_{0.87}$	205	7.06	6.00	8.26	17

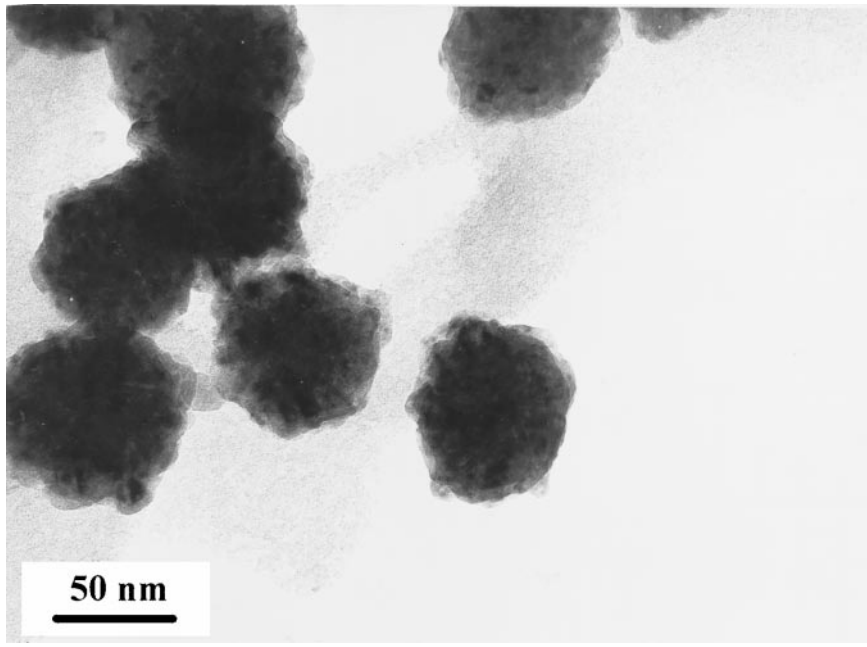

(a)

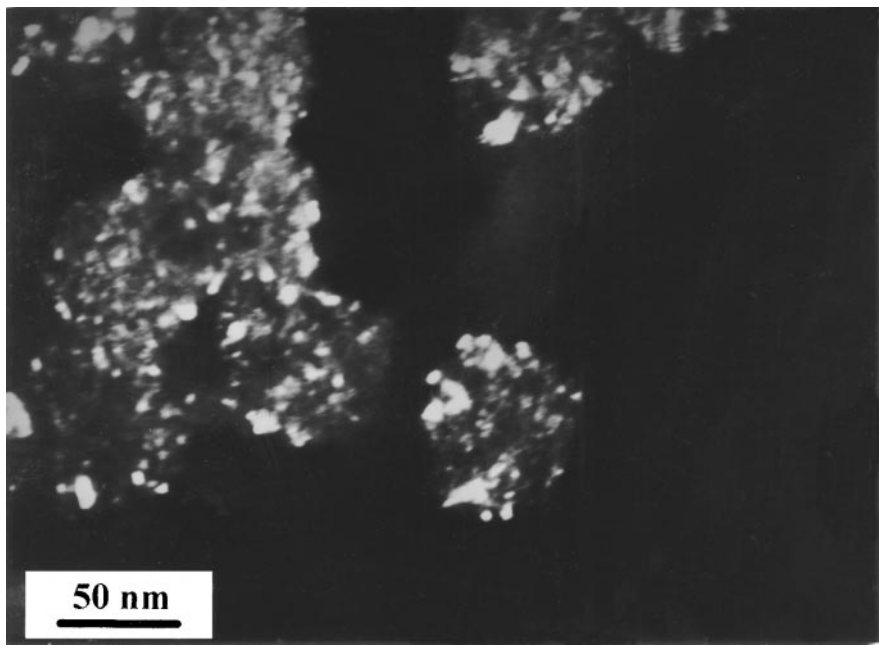

(b)

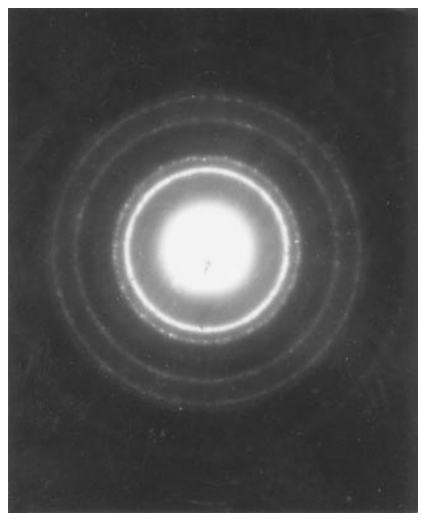

(c)

Figure 10 TEM (a) bright field and (b) dark-field micrographs, (c) SAED by an isolated particle for a $Fe_{0.13}[Co_{20}Ni_{80}]_{0.87}$ powder ($d_m = 75$ nm, $\sigma = 7$ nm).

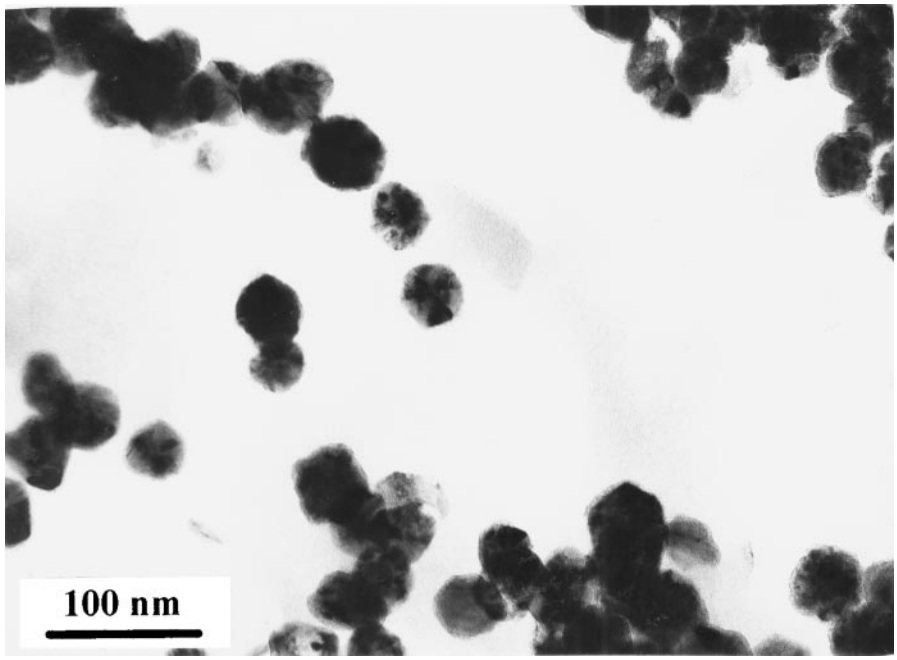

(a)

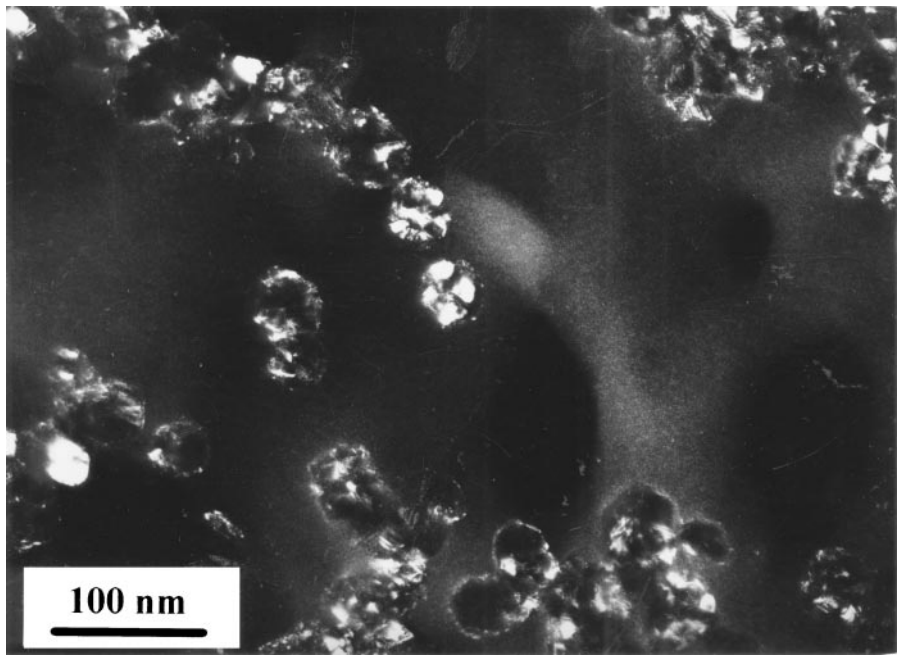

(b)

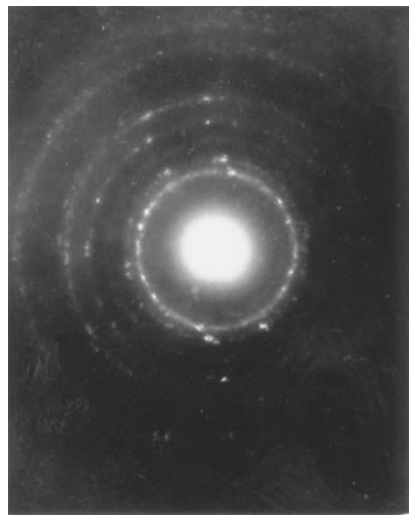

(c)

Figure 11 TEM (a) bright field and (b) dark-field micrographs, (c) SAED by an isolated particle for a $Co_{65}Ni_{35}$ powder ($d_m = 42$ nm, $\sigma = 5$ nm).

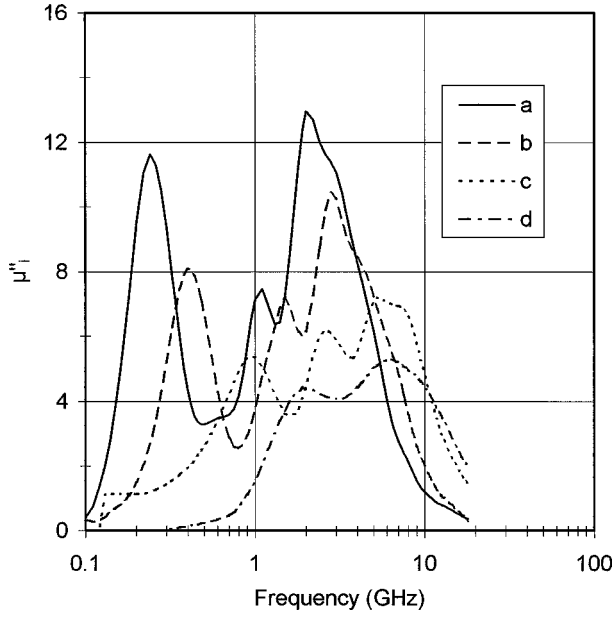

Figure 12 Imaginary part of the intrinsic permeability of $Fe_{0.13}[Co_xNi_{100-x}]_{0.87}$ powders for different compositions with an almost constant particle size: (a) $Fe_{0.13}[Co_{20}Ni_{80}]_{0.87}$, $d_m = 225$ nm; (b) $Fe_{0.13}[Co_{50}Ni_{50}]_{0.87}$, $d_m = 205$ nm; (c) $Fe_{0.13}[Co_{80}Ni_{20}]_{0.87}$, $d_m = 215$ nm; (d) $Fe_{13}Co_{87}$, polydisperse.

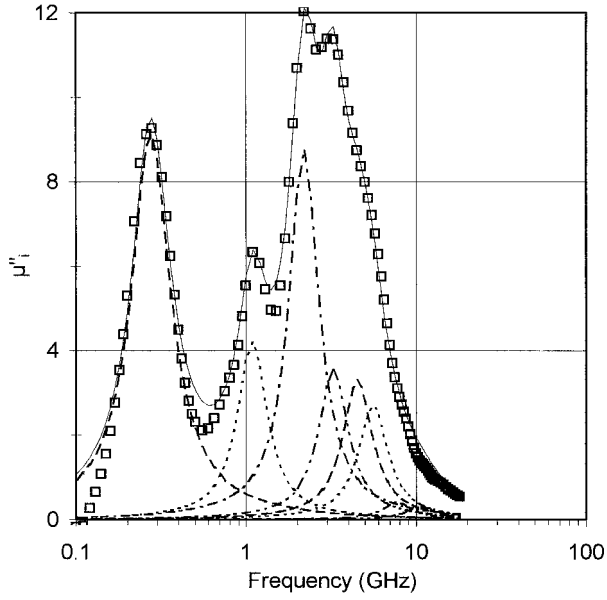

Figure 13 Decomposition of the imaginary part of the intrinsic permeability of FeCoNi particles as a sum of profiles resulting from the resolution of the Gilbert equation: (open squares) experimental values; (dashed lines) band profiles; (solid line) sum of profiles.

wide range of chemical composition. Previous studies [44] have established clearly that the permeability of cobalt-nickel particles with a mean diameter lower than 400 nm presents several resonance bands in the 0.1–18 GHz range. A similar effect is observed for iron-cobalt-nickel particles with a mean diameter in the 50–400 nm range (Fig. 12). For both Co_xNi_{100-x} and $Fe_z[Co_xNi_{100-x}]_{1-z}$ systems, the resonance modes are shifted toward high frequencies when the mean particle size decreases.

Beyond the size effect, a deeper analysis allows to evidence composition effects upon the microwave permeability of submicrometer-sized FeCoNi particles. As shown in Fig. 12, the multiresonant behavior appears for almost all $Fe_{0.13}[Co_xNi_{100-x}]_{0.87}$ samples and the resonance frequencies are shifted toward high frequencies when the cobalt content increases. It is noteworthy that the $Fe_{13}Co_{87}$ particles have to be distinguished from all the other compositions since their permeability curve presents two broad bands and a μ''_{max} value much lower than that reached for any other composition (Fig. 12).

The permeability curve of samples showing a multiresonant behavior can be fitted quite well by a sum of profiles resulting from the resolution of the Gilbert equation (see Appendix) as exemplified in Fig. 13. The reliability factor defined as $R = \sum_i [\mu_{exp}(i) - \mu_{calc}(i)]^2 / \sum_i [\mu_{exp}(i)]^2$ is found less than 5×10^{-3}. These decompositions provide the resonance frequencies f_i and the damping parameters α_i which are related to the broadening of the resonance bands (Equation 4a and b in Appendix). An accurate determination of these parameters can be done only for the four lower frequency resonance bands, the following ones being too low in intensity. For a given powder the damping parameter of the first mode α_1 is always found slightly higher than the following ones (Table VIII). In order to limit calculations the damping parameters of these upper modes α_2 were kept equal for a given powder. They are found almost constant for $Fe_{0.13}[Co_xNi_{100-x}]_{0.87}$ particles with a similar average diameter, for every composition except for the cobalt rich composition for which they are found higher (Table VIII).

The microwave properties of $Fe_{0.13}[Co_xNi_{100-x}]_{0.87}$ and Co_xNi_{100-x} particles with a similar mean diameter and a same x value have been compared (Fig. 14). It can be seen that an iron content as low as 13% by wt. modifies significantly the permeability of the ferromagnetic particles. Two effects can be noted: (i) the resonance bands appear at lower frequencies for the iron-based particles than for iron-free particles; (ii) the maxima of permeability reached with the iron-based particles are always higher than that reached with the cobalt-nickel particles (Table VIII). Nevertheless the α values of CoNi and FeCoNi samples having the same Co/Ni ratio are found very close (Table VIII).

Finally, the thermal treatments described above allow to increase the permeability levels, the resonance frequencies being only slightly modified (Fig. 15). This increase of μ''_{max} is quite limited between 15 and 20% for CoNi particles. It can be much more important for FeCoNi samples especially when they present a high impurities level and a polycrystalline state.

4.2. Discussion

The multiresonance observed with submicrometer-sized ferromagnetic particles was interpreted as non uniform resonance modes resulting from the exchange energy contribution to the magnetization precession within the particles. Such a contribution is expected to be effective only for thin samples and the frequency of these modes depends on the sample geometry. These exchange modes were extensively studied for thin films both from a theoretical and an experimental point of view. In case of spherical particles a theoretical

TABLE VIII Main features of the intrinsic permeability of the Co_xNi_{100-x} and $Fe_{0.13}[Co_xNi_{100-x}]_{0.87}$ particles: damping parameters α_1 and α_2 resulting from the profile fitting; agreement factor of the fitting defined as $R = \sum_i [\mu_{exp}(i) - \mu_{calc}(i)]^2 / \sum_i [\mu_{exp}(i)]^2$; maximum level of the imaginary part of the intrinsic permeability $\mu''_{i\max}$; value of the real part of the intrinsic permeability μ'_i at 0.1 GHz

Co_xNi_{100-x} particles					
x	80	50	35	20	0
d_m (nm)	220	250	210	250	220
α_1	0.52	0.43	0.38	0.36	
α_2	0.25	0.25	0.25	0.275	
R	1.5×10^{-3}	1.5×10^{-3}	3.10^{-3}	2.5×10^{-3}	
$\mu''_{i\max}$	6.6	8.7	9.5	9	4.9
μ'_i (0.1GHz)	8.9	10.7	12.6	12.6	7.1
$Fe_{0.13}[Co_xNi_{100-x}]_{0.87}$ particles					
x	80	50	35	20	0
d_m (nm)	215	205	245	225	≈200
α_1	0.65	0.37	0.335	0.375	
α_2	0.3	0.25	0.25	0.25	
R	2×10^{-3}	2×10^{-3}	3×10^{-3}	1.5×10^{-3}	
$\mu''_{i\max}$	7.2	10.4	12.0	12.9	14.4
μ'_i (0.1 GHz)	17.2	17.1	19.9	22.7	

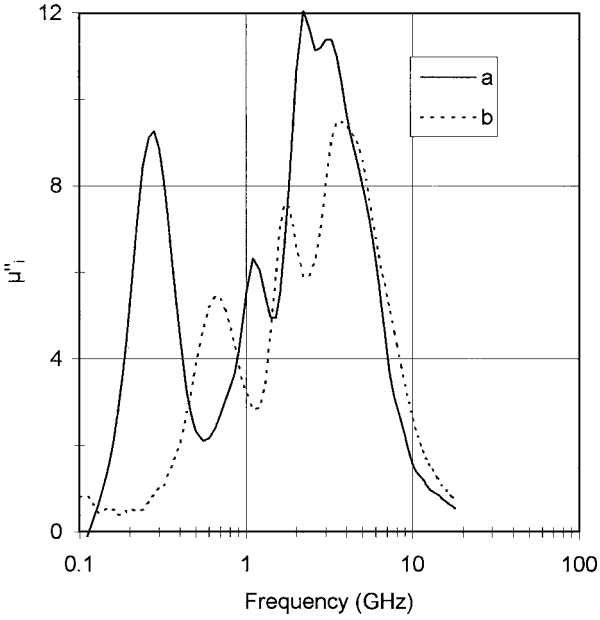

Figure 14 Influence of iron content upon permeability for two powders with an almost constant particles size: (a) $Fe_{0.13}[Co_{35}Ni_{65}]_{0.87}$, d_m = 245 nm; (b) $Co_{35}Ni_{65}$, $d_m = 225$ nm.

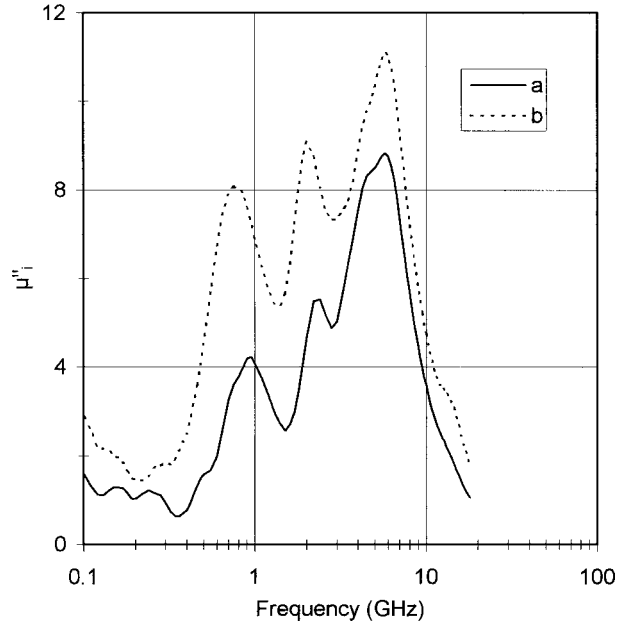

Figure 15 Imaginary part of the intrinsic permeability of a $Co_{50}Ni_{50}$ powder ($d_m = 190$ nm) (a) before and (b) after thermal treatment.

expression of these modes was given by Aharoni [45]. For such a particle shape the frequencies of the exchange resonance modes, f_{kn}, are expected to follow the general formula:

$$f_{kn} = \gamma \frac{C\mu_{kn}^2(R)}{R^2 M_S} + f_1 \qquad (3)$$

with C the exchange constant, γ the gyromagnetic ratio, R the particle radius, M_s the saturation magnetization and f_1 the uniform resonance mode frequency which depends on the magnetocrystalline anisotropy. In absence of surface anisotropy the eigenvalues μ_{kn} are constants and do not depend on the particle size. If a surface anisotropy is taken into account Aharoni showed than these eigenvalues μ_{kn} become size dependent and therefore the resonance frequencies dependence upon R is expected to be significanlty modified [46].

The study of the particle size influence on the permeability allowed us to show that: (i) the first band frequency is poorly dependent on the particle size all over a large range [21]; (ii) the eigenvalues μ_{kn} calculated by Aharoni for the spherical geometry described quite well the frequency dispersion [20]. Thus it is possible to use the Aharoni theory as a guideline for the interpretation of the permeability of fine spherical particles. The first band is mainly related to the magnetocrystalline anisotropy of the particles. The following ones strongly depend on the particle mean radius with the C/M_s ratio as coefficient. The R^{-1} dependence of these bands frequencies observed experimentally [20] can be tentatively explained, according to Aharoni, by a surface anisotropy related to the core-shell texture described in the first part of this paper. The overall shift of the resonance bands toward high frequencies which is observed

when the Co content increases for both Co_xNi_{100-x} and $Fe_z[Co_xNi_{100-x}]_{1-z}$ systems is related to an increase of the magnetocrystalline anisotropy as it is observed for CoNi bulk alloys when the Co content increases [38]. Moreover the shift of the resonance bands toward low frequencies for the FeCoNi particles respected to the CoNi particles with the same Co/Ni ratio has to be interpreted as the consequence of a lowering of the magnetic anisotropy with the introduction of small amount of iron in the lattice.

If the resonance frequencies dependence upon size and in some extent upon chemical compositions is now quite well understood, the factors acting upon the permeability levels and the band broadening have been less studied. The large variety of characteristics of the particles investigated in the present study makes possible a qualitative discussion about the influence on these two factors of both the intrinsic magnetic properties and the structural and textural characteristics of the particles described above.

At first it must be stressed that an important cause of broadening, if not the main, is independent of the particle characteristics but results from the random dispersion of the particles, as in every resonance experiments. Nevertheless, the band broadening is also related to the morphology of the particles. With powders made up of particles with poorly defined shapes, one can expect nothing else that a very broad resonance band because of the effect of the demagnetizing fields which are related to the particle shape. Moreover for particles with a uniform shape, the resonance bands will be broaden by the size distribution as it can be easily inferred from Equation 3. The very broad bands and the low μ'' level observed with FeCo particles have to be interpreted as a consequence of the various shapes and of the broad size distribution of these particles. For all other compositions the particles are spherical and monodisperse and their permeability curves present much more narrow bands.

Other factors which can act upon the band broadening are the structural and textural characteristics of the particles. It has been shown above that the Ni rich CoNi and FeCoNi particles crystallize as a single fcc phase. For Co rich CoNi particles a further hcp phase is observed and a third bcc phase appears when $x > 80$ in the $Fe_z[Co_xNi_{100-x}]_{1-z}$ system. The larger broadening observed on the permeability curves of monodisperse Co rich FeCoNi particles (Table VIII) may be related to the structural heterogeneity of these particles. For the other compositions the damping parameters α_i are found almost independent of the composition, even for the Co rich CoNi particles (Table VIII). One can conclude that the occurrence of a mixture of close-packed phases (fcc and hcp) do not cause any supplementary broadening with respect to a single fcc phase. Moreover the lower crystallinity (smaller crystallite size, porosity) of the iron-based particles with respect to the CoNi particles with the same Co/Ni ratio (see above) does not contribute in a significant way to the band broadening.

Annealing has for consequence to increase the permeability level. Among the different factors which can affect the permeability level of a composite materials, the most trivial is the volume concentration of the magnetic part in the composite. Thus, it is not surprising that the permeability levels increase after a thermal treatment of the ferromagnetic particles since such a treatment results in a decrease of the impurity contents.

To our knowledge, no theoretical expressions of the band intensity and broadening of non uniform modes are available for the moment for spherical particles. Nevertheless, it is well known that whatever the dissipation mechanism, the magnetic losses (and thus the intensity of the imaginary part of the dynamic permeability) within the material are related to the static permeability. Moreover, the permeability levels are also related to the band broadening (Equation 6 in Appendix). We saw above that the introduction of small amounts of iron in the particle composition allowed to reach higher levels of permeability. These higher μ''_{max} values reached by the FeCoNi particles with respect to CoNi particles can not be related to a lower broadening of the resonance bands since the damping parameters are found constant for most of CoNi and FeCoNi compositions (Table VIII). At the opposite the iron based particles present values of the real part of the permeability μ' at 100 MHz always higher than 15 whereas those of the cobalt-nickel particles are always lower (Table VIII). Therefore the higher μ''_{max} values reached by the FeCoNi particles can be related to this higher initial permeability. It is commonly accepted that the static permeability of fine particles is limited to a rotational permeability since no magnetic wall excitations can take place within the particles. The static susceptibility, χ_0, is equal to the M_s/H_0 ratio, M_s being the magnetization saturation and H_0 the internal field. Without any applied static field the internal field can be taken as H_a, the anisotropy field. Thus in that latter case μ''_{max} is expected to be proportional to the M_s/H_a ratio or to the M_s^2/K_1 ratio with K_1 the anisotropy constant. Hence the increase of the permeability levels of iron-based particles with respect to iron-free ones can be interpreted as the consequence of two effects: a decrease of the anisotropy (which produces also a shift of the resonance bands toward the low frequencies) and an increase of the saturation magnetization of the ferromagnetic moiety of the particles.

5. Conclusion

Co-Ni and Fe-Co-Ni powders made by the polyol process have a set of morphological characteristics (a quasi-spherical particle shape, a controllable submicrometer particle size, a narrow size distribution) which make the study of their dynamic magnetic properties of particular interest. In both systems the microwave permeability of submicrometer sized particles shows several narrow bands, the lower frequency one being considered as a uniform resonance mode which does not depend on the particle size, and the others as non-uniform exchange resonance modes whose frequencies are size-dependent. This microwave resonance behavior varies also with the composition of the metal powders, the resonance frequencies being related to the magnetocrystalline anisotropy and the maximum

permeability level being higher for iron-based particles than for iron-free ones. In both systems particles are made up by a metallic core coated by a thin layer of non metallic impurities. The number of metallic phases observed in the metallic core of the particles and their cristallinity vary also with composition. Except for powders of particular compositions characterized by a high structural heterogeneity or a very low cristallinity these structural and textural characteristics have not a very strong influence on the resonance behavior. Thus, despite their lower cristallinity and their higher impurity contents iron-based particles show the highest permeability levels which can be still increased by thermal treatments. After annealing, such iron-based particles appear particularly suitable to be used as magnetic inclusions to make granular materials with optimized and controllable absorption characteristics.

Appendix

The Gilbert modification of the Landau-Lifshitz equation is often used to describe a resonance process when the damping is large [47]. The resolution of this equation leads in the isotropic case to the susceptibility, χ, as a function of the frequency; the real and imaginary part of this susceptibility being respectively:

$$\chi' = \chi_0 \frac{\left[1-(f/f_0)^2(1-\alpha^2)\right]}{\left[1-(f/f_0)^2(1+\alpha^2)\right]^2+4\alpha^2(f/f_0)^2} \quad (4a)$$

$$\chi'' = \chi_0 \frac{(f/f_0)\alpha\left[1+(f/f_0)^2(1+\alpha^2)\right]}{\left[1-(f/f_0)^2(1+\alpha^2)\right]^2+4\alpha^2(f/f_0)^2} \quad (4b)$$

with f the frequency, f_0 the resonance frequency, α a damping constant and χ_0 the static susceptibility. The damping constant is linked to the full width half height Δf by the relation:

$$2\alpha = \frac{\Delta f}{f_0} \quad (5)$$

The permeability μ is related to the susceptibility by the relation: $\mu = 1+\chi$. (S.I. units) From Equation 4b it can be inferred when α is not too large that the μ'' value at the resonance is given by:

$$\mu''_{\text{max.}} = \frac{\chi_0}{2\alpha} \quad (6)$$

The multi-resonant permeability vs. frequency curves can be tentatively fitted by a sum of curves described in Equation 4. In that case the static susceptibility is replaced by an adjustable parameter I which is the intensity of the band. The whole curve is thus fitted by the following function:

$$\mu'' = \sum_i I_i \frac{(f/f_i)\alpha_i\left[1+(f/f_i)^2\left(1+\alpha_i^2\right)\right]}{\left[1-(f/f_i)^2\left(1+\alpha_i^2\right)\right]^2+4\alpha_i^2(f/f_i)^2} \quad (7)$$

Acknowledgements

The authors are indebted to L. Lesage, M.-J. Vaulay and G. Cheguillaume for their contribution to materials characterization.

References

1. E. MATIJEVIC, *Faraday Discuss.* **92** (1991) 229.
2. W. WERNSDORFER, E. B. OROZCO, B. BARBARA, K. HASSELBACH, A. BENOIT, D. MAILLY, B. DOUDIN, J. MEIER, J. E. WEGROWE, J.-P. ANSERMET, N. DEMONCY, H. PASCARD, A. LOISEAU, L. FRANCOIS, N. DUXIN and M.-P. PILENI, *J. Appl. Phys.* **81** (1997) 5543.
3. K. V. P. M. SHAFI, A. GEDANKEN and R. PROZOROV, *Adv. Mater.* **10** (1998) 590.
4. B. MORTEN, M. PRUDENZIATI, G. DE CICCO, A. BIANCO, G. MONTESPERELLI and G. GUSMANO, *Meas. Sci. Technol.* **8** (1997) 21.
5. H. PASTOR, M. BONNEAU and J. PILOT, in International Conference on Advances in Hard Materials Production, Bonn, 1992.
6. S. GANGOPADHYAY, Y. YANG, G. C. HADJIPANAYIS, V. PAPAEFTHYMIOU, C. M. SORENSEN and K. J. KLABUNDE, *J. Appl. Phys.* **76** (1994) 6319.
7. X. BAO, F. LI and R. M. METZGER, *ibid.* **79** (1996) 4866.
8. C. F. KERZNIZAN, K. J. KLABUNDE, C. M. SORENSEN and G. C. HADJIPANAYIS, *ibid.* **67** (1990) 5897.
9. S. EROGLU, S. C. ZHANG and G. L. MESSING, *J. Mater. Res.* **11** (1996) 2131.
10. K. V. P. M. SHAFI, A. GEDANKEN and R. PROZOROV, *J. Mater. Chem.* **8** (1998) 769.
11. M. RESPAUD, J. M. BROTO, H. RAKOTO, A. R. FERT, L. THOMAS, B. BARBARA, M. VERELST, E. SNOECK, P. LECANTE, A. MOSSET, J. OSUNA, T. OULD ELY, C. AMIENS and B. CHAUDRET, *Phys. Rev. B* **57** (1998) 2925.
12. R. S. SAPIESZKO and E. MATIJEVIC, *Corrosion* **36** (1980) 522.
13. F. FIEVET, J.-P. LAGIER and M. FIGLARZ, in Proceedings of the Powder Metallurgy World Congress, Paris, June 1994 (Les Editions de Physique, Les Ulis, 1994) Vol. 1, p. 281.
14. J. P. CHEN, C. M. SORENSEN, K. J. KLABUNDE and G. C. HADJIPANAYIS, *J. Appl. Phys.* **76** (1994) 6316.
15. C. PETIT, A. TALEB and M.-P. PILENI, *J. Phys. Chem. B* **103** (1999) 1805.
16. F. FIEVET, J.-P. LAGIER, B. BLIN, B. BEAUDOIN and M. FIGLARZ, *Solid State Ionics* **32/33** (1989) 198.
17. G. VIAU, F. FIEVET-VINCENT and F. FIEVET, *J. Mater. Chem.* **6** (1996) 1047.
18. G. VIAU, Ph.D. thesis, Paris 7-Denis Diderot University, Paris, 1995.
19. PH. TONEGUZZO, Ph.D. thesis, Paris 7-Denis Diderot University, Paris, 1997.
20. G. VIAU, F. FIEVET-VINCENT, F. FIEVET, PH. TONEGUZZO, F. RAVEL and O. ACHER, *J. Appl. Phys.* **81** (1997) 2749.
21. PH. TONEGUZZO, G. VIAU, O. ACHER, F. FIEVET-VINCENT and F. FIEVET, *Adv. Mater.* **10** (1998) 1032.
22. M. KISHIMOTO, S. KITAHATA and M. AMEMIYA, *IEEE Trans. Magn.* **22** (1986) 732.
23. A. M. HOMOLA, M. R. LORENZ, C. J. MASTRANGELO and T. L. TILBURY, *ibid.* **22** (1986) 716.
24. T. ISHIKAWA and E. MATIJEVIC, *Langmuir* **4** (1988) 26.
25. L. KOCON, H. LACAMPAGNE and P. LATARE, in Proceedings of the Powder Metallurgy World Congress, Paris, June 1994 (Les Editions de Physique, Les Ulis, 1994) Vol. 3, p. 1823.
26. H. P. KLUG and L. E. ALEXANDER, in "X-Ray Diffraction Procedures for Polycrystalline and Amorphous Materials," 2nd Ed. (John Wiley & Sons, New York, 1974) Ch. 8, p. 566.
27. G. K. WILLIAMSON and W. H. HALL, *Acta Metal.* **1** (1953) 22.
28. F. E. LUBORSKI, *J. Appl. Phys.* **32** (1961) 1715.
29. S. GANGOPADHYAY, G. C. HADJIPANAYIS, C. M. SORENSEN and K. J. KLABUNDE, *IEEE Trans. Magn.* **28** (1992) 3174.

30. Y. LI, W. GONG, G. C. HADJIPANAYIS, C. M. SORENSEN, K. J. KLABUNDE, V. PAPAEFTHYMIOU, A. KOSTIKAS and A. SIMOPOULOS, *J. Magn. Magn. Mat.* **130** (1994) 261.
31. G. C. HADJIPANAYIS, S. GANGOPADHYAY, L. YIPING, C. M. SORENSEN and K. J. KLABUNDE, in "Science and Technology of Nanostructured Magnetic Materials," edited by G. C. Hadjipanayis and G. A. Prinz (Plenum Press, New York, 1991) p. 497.
32. S. GANGOPADHYAY, G. C. HADJIPANAYIS, C. M. SORENSEN and K. J. KLABUNDE, *IEEE Trans. Magn.* **29** (1993) 2602.
33. F. T. PARKER and A. E. BERKOWITZ, *Phys. Rev. B* **44** (1991) 7437.
34. S. GANGOPADHYAY, G. C. HADJIPANAYIS, B. DALE, C. M. SORENSEN, K. J. KLABUNDE, V. PAPAEFTHYMIOU and A. KOSTIKAS, *ibid.* **45** (1992) 9778.
35. "Handbook of Chemistry and Physics," 76th ed., edited by D. R. Lide (C.R.C. Press, New-York, 1995–96).
36. I. TAMURA and M. HAYASHI, *Surf. Sci* **146** (1984) 501.
37. T. SHINJO, T. SHIGEMATSU, N. HOSAITO, T. IWASAKI and T. TAKAI, *Jpn. J. Appl. Phys.* **21** (1980) L220.
38. LANDOLT-BÖRNSTEIN, in "Magnetic Properties," New Series III/19A (Springer, Berlin, 1982).
39. A. TAYLOR, *J. Inst. Metals* **77** (1950) 585.
40. X ray powder data file J.C.P.D.S., No.4-850, No. 15-806.
41. "Constitution of Binary Alloys," 2nd ed., edited by M. Hansen, R. P. Helliot and K. Anderkop (McGraw Hill, New York, 1985) and Refs therein.
42. M. FIGLARZ, F. VINCENT, C. LECAILLE and J. AMIEL, *Powder Technol.* **1** (1967) 121.
43. G. VIAU, F. FIEVET-VINCENT and F. FIEVET, *Solid State Ionics* **84** (1996) 259.
44. PH. TONEGUZZO, O. ACHER, G. VIAU, F. FIEVET-VINCENT and F. FIEVET, *J. Appl. Phys.* **81** (1997) 5546.
45. A. AHARONI, *ibid.* **69** (1991) 7762.
46. *Idem.*, *ibid.* **81** (1997) 830.
47. *Idem.*, in "Introduction to the Theory of Ferromagnetism" (Clarendon Press, Oxford, 1996), Ch. 8, p. 181.

Received 11 August
and accepted 10 December 1999